Available online at www.sciencedirect.com
ScienceDirect
Optik 120 (2009) 121–126
Optik Optics
www.elsevier.de/ijleo

Effect of oxide aperture on the performance of 850 nm vertical-cavity surface-emitting lasers

A. Mohd Sharizal[a], Paul O. Leisher[b], Kent D. Choquette[b], P.K. Choudhury[c,*], Sufian M. Mitani[a], Y. Mohd Razman[a], A.M. Abdul Fatah[a]

[a]*Telekom Research & Development (TMR&D), Idea Tower, UPM-MTDC, Lebuh Silikon, 43400 Serdang, Selangor, Malaysia*
[b]*Electrical & Computer Engineering Department, University of Illinois at Urbana-Champaign (UIUC), Urbana, 61801 IL, USA*
[c]*Faculty of Engineering, Multimedia University, 63100 Cyberjaya, Selangor, Malaysia*

Received 12 March 2007; accepted 30 July 2007

Abstract

An experimental study has been presented of the oxide-confined vertical-cavity surface-emitting lasers (VCSELs) operating in the 850 nm region of the electromagnetic spectrum. In this regard, various relevant VCSEL samples with numerous oxide aperture sizes have been fabricated and characterized. Thorough investigations of the electrical as well as optical characteristics of the fabricated samples have been performed, which include the overall device performance as a function of the oxidize aperture sizes. It is reported that the VCSELs with oxide aperture size $<10\,\mu m$ require low threshold currents (<1 mA). Further, the differential quantum efficiencies up to 28% corresponding to wall-plug efficiencies of up to 15% were measured for a number of these devices.

Keywords: VCSELs; Multiple layer propagation

1. Introduction

Investigators have shown continued interest in the development of various types of vertical-cavity surface-emitting lasers (VCSELs) and their specific applications owing to their stable temperature dependence and high-speed operation in data transmission [1–6]. Depending on the requirements, VCSELs are invented according to the desirable operating wavelength [7,8]. Sophisticated design of VCSELs includes surface emission with high spectral performance, which makes the 2D array integration simpler, reducing thereby the manufacturing cost of the device.

VCSELs with operating wavelengths at 850 nm are now widely used for short-haul optical communications, and have dominated the semiconductor laser applications. Successful research in this area could now develop a standard technology to commercialize the applications of 850 nm VCSELs in low-cost optical links and local area networks [9,10]. In order to improve the device performance at this wavelength, various techniques such as oxide confinement [11], surface-relief etching [12], extended optical cavity [13], increased fundamental mode gain [14], hybrid implant/oxide structure [15], composite resonators [16], etc. are implemented.

Fabrication of distributed Bragg reflectors (DBRs), which are multilayered waveguides, plays an important role in determining the performance of a VCSEL device. Therefore, different parameters related to the DBRs,

*Corresponding author. Fax: +60 3 8318 3029.
E-mail address: pankaj@mmu.edu.my (P.K. Choudhury).

0030-4026/$ - see front matter © 2007 Elsevier GmbH. All rights reserved.
doi:10.1016/j.ijleo.2007.07.005

including the type of materials used for DBR fabrication, play vital roles in determining the emission wavelength [10,17]. Choudhury and Singh [18] worked extensively on such multilayered waveguides. Mitani et al. recently reported the characteristic features of some new type of VCSELs with [19,20] and without [21] oxide confinement layers. However, their analyses were based on simulation methods, and it was reported that the proposed design could result in efficient operation of the VCSEL in the 850 nm region.

In the present paper, the authors aim to present the characteristic features of oxide confined 850 nm VCSELs with various oxide aperture sizes. For this, VCSEL devices with various etched mesa sizes and corresponding oxide aperture sizes are fabricated. The light–current (L–I) and current–voltage (I–V) characteristics for each of these devices are measured. This way a study has been presented of the device performance in respect of the dependence of their efficiencies (such as differential quantum efficiency and wall-plug efficiency) and spectral characteristics on the size of the oxide aperture. The results indicate the growth of high-quality epiwafer finally resulting in successful fabrication of efficient 850 nm VCSELs. Low threshold current and low differential series resistance are observed for the fabricated devices. Further, the output spectral characteristics indicate typical multimode operation for these devices.

2. The device and its fabrication

Fig. 1 shows the schematic diagram of a single 850 nm VCSEL device. The fabricated VCSEL epiwafer structure has 34.5 periods of n-type and 24.5 periods of p-type DBRs at the bottom and the top, respectively. Also, three GaAs quantum wells, sandwiched between top and bottom DBRs, serve the purpose of an active region for the VCSEL. Both the DBRs are composed of alternating high and low refractive index (RI) layers of $Al_{0.9}Ga_{0.1}As/Al_{0.15}Ga_{0.85}As$. Further, in order to achieve selective oxidation, one layer of $Al_{0.98}Ga_{0.02}As$ is introduced underneath the top p-DBR. All the layers

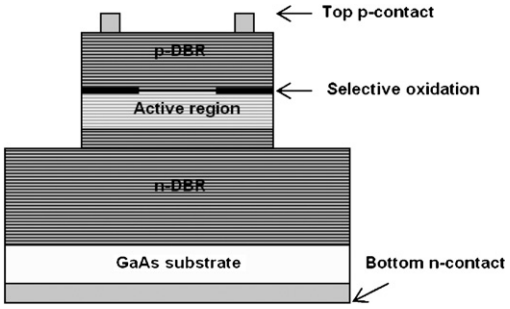

Fig. 1. Schematic of 850 nm VCSEL device.

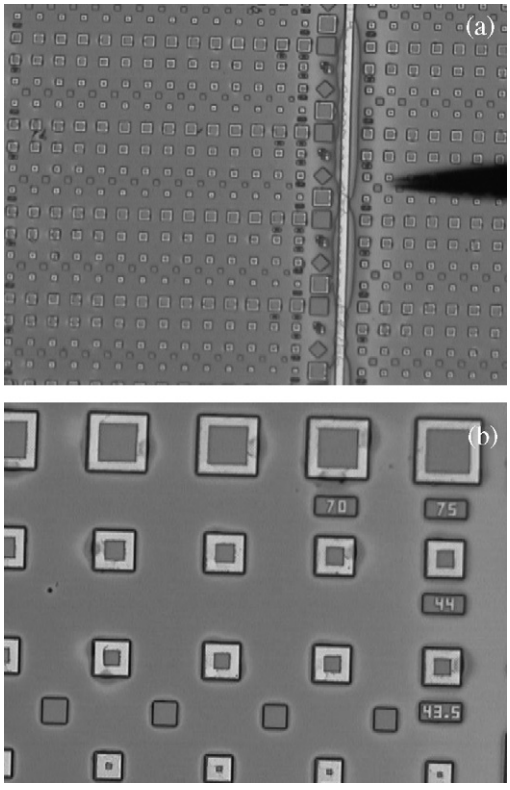

Fig. 2. (a) Various fabricated 850 nm VCSEL devices; (b) larger view of VCSEL mesa sizes.

are grown by the process of metal-organic chemical vapor deposition. In order to investigate the device efficiency and spectral characteristics as a function of the size of the oxide aperture, numerous mesa structures (and corresponding oxide aperture sizes) are fabricated from this epiwafer.

The fabrication begins with the definition of a top ring contact pattern using standard optical lithography. In order to form ohmic contacts for the p-type DBR, Ti/Au (15 nm/150 nm) layers are evaporated, and then lifted off. The evaporation of AuGe/Ni/Au (40 nm/20 nm/150 nm) forms the ohmic contact for the n-type DBR. The process of evaporation involves both thermal and electron beam evaporations. In order to isolate various VCSEL devices and expose the high RI Al-layer for oxidation, mesa structures are developed. Thus, the mesa structures essentially have dual purpose. The technique includes the deposition of SiO_2 layer by the process of plasma-enhanced chemical vapor deposition. Such a dielectric layer is then patterned by using standard optical lithography and CF_4 reactive ion etching (RIE). This patterned dielectric is used as the mask for the mesas that are etched by inductively coupled plasma RIE. The high RI Al-layer is then selectively oxidized by wet oxidation to define the oxide aperture, and the SiO_2 mesa mask is removed by the process of CF_4 RIE. Since the rate of oxidation is independent of mesa size, each of the different mesas

uniquely corresponds to one particular value of the oxide aperture size. Fig. 2 illustrates VCSEL devices with different mesas (and with different oxide aperture sizes) fabricated on a single VCSEL epiwafer sample. This is done for studying the VCSEL device efficiency and spectral characteristics as a function of oxide aperture size.

3. Experimental results and discussion

In our experiment, we perform on-wafer probing measurements for obtaining the light–current (L–I) and current–voltage (I–V) characteristics of the fabricated VCSELs. Electrical contact to the VCSEL is established by probing the top DBR, with the backside of the sample grounded through the probe station chuck (Fig. 3). A Keithley 236 DC current source is used to supply current. A precise variation of the injection current is achieved by using an Agilent 4156C semiconductor parameter analyzer. In order to determine the output optical power, the lasing VCSEL is detected by a Si-photodetector, which is also connected to the semiconductor parameter analyzer. Spectral properties of the device are analyzed by coupling the lasing VCSEL beam into a multimode optical fiber (through a suitable microscope objective), which is connected to an Agilent 86141B optical spectrum analyzer.

Fig. 4 illustrates the L–I characteristics of VCSELs having various etched mesa sizes. In order to determine the dimensions of the oxide apertures, electrical probing was used to test which of the mesa sizes are not conducting (pinched-off). We noticed that the VCSELs with mesa size $27 \times 27\,\mu m^2$ and below were pinched-off. Thus, in our experiment, each of the VCSEL mesas with sizes 30×30, 36×36, 45×45, 62×62 and $75 \times 75\,\mu m^2$ have their respective oxide aperture sizes of 3×3, 9×9, 18×18, 35×35 and $48 \times 48\,\mu m^2$. We observe from

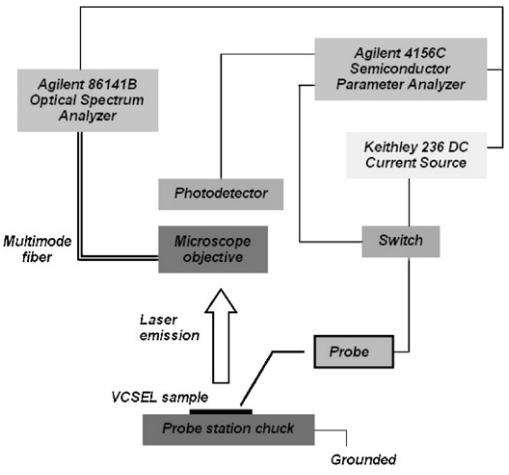

Fig. 3. The experimental measurement setup.

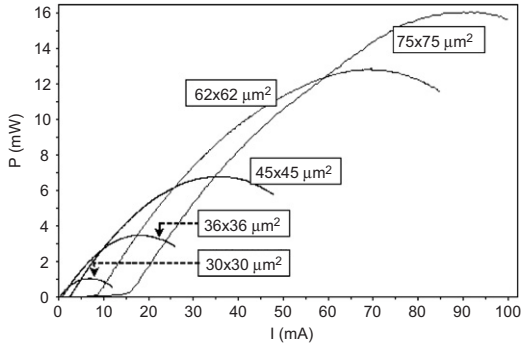

Fig. 4. L–I characteristics of fabricated VCSEL devices with various mesa sizes.

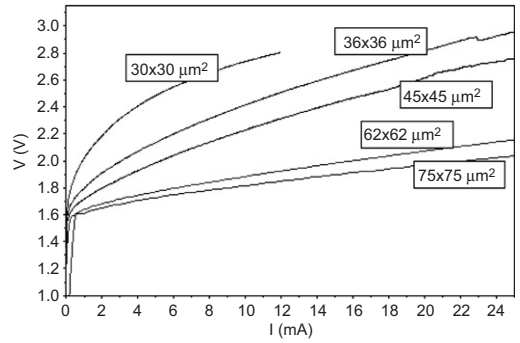

Fig. 5. I–V characteristics of fabricated VCSEL devices with various mesa sizes.

Fig. 4 that the threshold currents and the maximum output powers for the different VCSELs range from 0.5 to 15 mA and 0.9 to 16 mW, respectively. The requirement of higher threshold current with increasing mesa size is very much expected. Since larger mesas will essentially have larger size of the oxide apertures (which define the lasing modes), a higher amount of output optical power is obtained with the increasing mesa size (owing to increased active region area in this case). The I–V characteristics for the fabricated VCSELs for different mesa sizes are shown in Fig. 5. We notice that, with the increase in mesa size, the slope of the I–V curve decreases, indicating thereby a reduction in differential series resistance, which is due to the increased value of the cross-sectional area of the oxide aperture.

The differential series resistance R_S can be obtained from the slope of the I–V curve. In general, as compared to other semiconductor laser diodes, VCSELs exhibit high series resistances owing to the steep heterojunction barriers of the multiple DBR interfaces. The variation of R_S and the maximum output power as functions of oxide aperture size are, respectively, shown in Figs. 6 and 7. We observe that the maximum output power increases with increasing values of the VCSEL aperture. This is attributed to the fact that, in larger oxide apertures, more lasing modes are being confined.

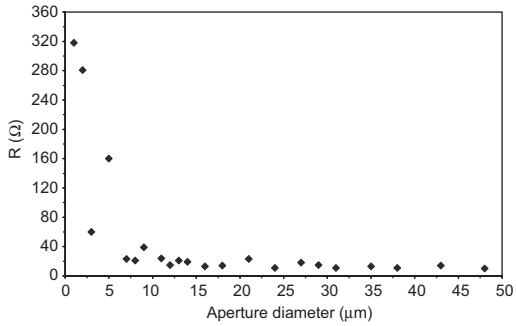

Fig. 6. Variation of differential series resistance with aperture size.

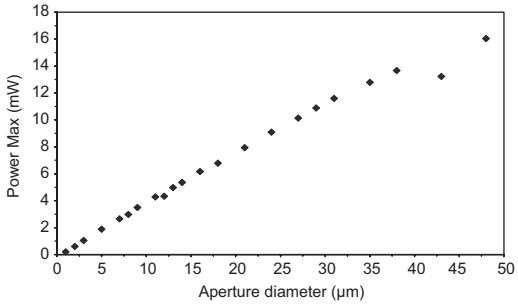

Fig. 7. Variation of maximum output power with aperture size.

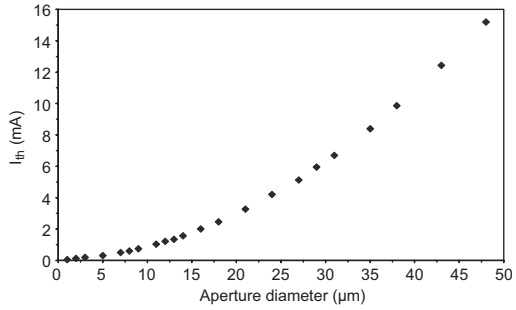

Fig. 8. Variation of threshold current with aperture size for fabricated VCSELs.

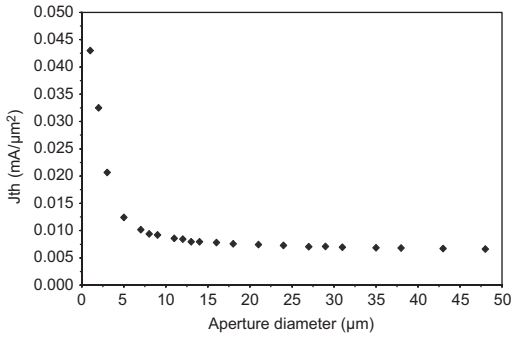

Fig. 9. Variation of threshold current density with aperture size.

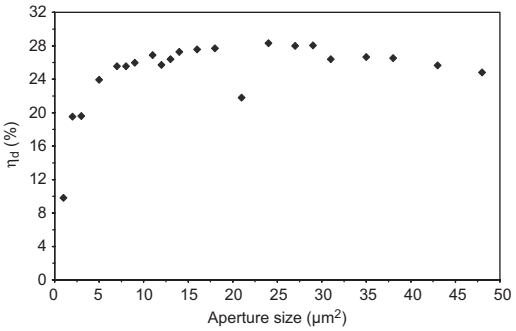

Fig. 10. Plot of differential quantum efficiency with various oxide apertures.

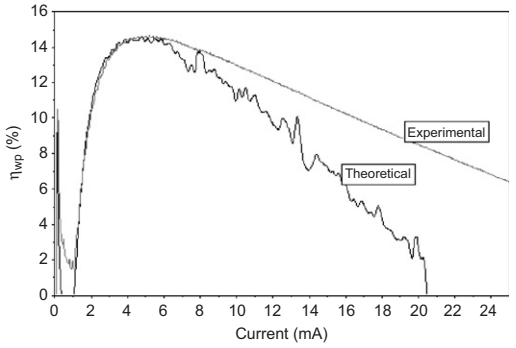

Fig. 11. Plot of wall-plug efficiency with input current for a VCSEL with $11 \times 11\,\mu m^2$ oxide aperture size.

Further, the inverse dependence of series resistance on VCSEL aperture size (Fig. 6) is due to the increased size of the conductive cross-sectional area, which is in agreement with Ohm's law.

Variation of the required threshold current I_{th} (Fig. 8) and that of the threshold current density J_{th} (Fig. 9) are also plotted as functions of oxide aperture size. Since the laser threshold gain essentially depends on threshold current density, as opposed to total threshold current, higher injection current is required for VCSELs with larger aperture sizes to achieve lasing operation. Further, since VCSEL devices were fabricated on the same wafer and processed in parallel, the threshold gain, and therefore the threshold current density, should remain constant theoretically regardless of the aperture size. From Fig. 9, we observe a kind of deviation from this fact for small oxide apertures, viz. 3×3–$10 \times 10\,\mu m^2$. This is primarily attributed to the increased optical scattering loss in the case of small-sized oxide apertures.

The differential quantum efficiency η_d indicates the efficiency of a VCSEL in converting the injected electron–hole pairs into photons emitted from the device. Fig. 10 illustrates the variation of η_d with the

oxide aperture sizes ranging from 1×1 to $48 \times 48\,\mu m^2$. We observe that the VCSELs with smaller oxide apertures show decreased differential quantum efficiency, which is due to the increased scattering loss resulting from the small oxide apertures.

The plot of wall-plug efficiency η_{wp} as a function of input current is shown in Fig. 11 from theoretical calculation [22] and experimental data. In this case, a typical example of the VCSEL with $11 \times 11\,\mu m^2$ oxide aperture size is considered. The wall-plug efficiency indicates the extent of the total input electrical power converted into the output optical power. We observe that a maximum wall-plug efficiency of 14.5% is achieved for the VCSEL sample under consideration.

4. Conclusion

The electro-opto characteristics of VCSELs fabricated on the same 850 nm epiwafer with various oxide aperture sizes are presented. The results reveal high efficiencies of the fabricated VCSEL devices, indicating thereby high-quality epiwafer growth. Low threshold current requirement and low differential series resistance are the real essence for the fabricated structures. Also, details of device efficiency such as differential quantum efficiency and wall-plug efficiency are studied, showing fabrication of efficient VCSEL devices.

Acknowledgments

The work is sponsored by Telekom Malaysia Berhad through the Project no. R05-0604-0. We are grateful to the researchers and the management of the Telekom Research & Development for technical aid and constant support. Also, we would like to acknowledge the Photonics Device Research Group of the University of Illinois at Urbana-Champaign for scientific collaboration during the project.

References

[1] J.Y. Law, G.P. Agrawal, Effects of spatial hole burning on gain switching in vertical-cavity surface-emitting lasers, IEEE J. Quantum Electron. 33 (1997) 462–468.

[2] C. Degen, I. Fischer, W. Elsässer, Transverse modes in oxide confined VCSELs: influence of pump profile, spatial hole burning, and thermal effects, Opt. Exp. 5 (1999) 38–47.

[3] J. Piprek, P. Abraham, J.E. Bowers, Self-consistent analysis of high-temperature effects on strained-layer multiquantum-well InGaAsP-InP lasers, IEEE J. Quantum Electron. 36 (2000) 366–374.

[4] F.H. Peters, M.H. MacDougal, High-speed high-temperature operation of vertical-cavity surface-emitting lasers, IEEE Photon. Technol. Lett. 13 (2001) 645–647.

[5] Y.S. Chang, H.C. Kuo, F.I. Lai, Y.A. Chang, L.H. Laih, S.C. Wang, Improvement of high speed performance for 10-Gb/s 850-nm VCSELs using InGaAsP/InGaP strain-compensated MQWs, Proc. SPIE 5364 (2004) 221–226.

[6] A.N. Al-Omari, K.L. Lear, High-speed, polymide vertical-cavity surface emitting lasers, Proc. SPIE 5364 (2004) 73–79.

[7] C.W. Wilmsen, Vertical-cavity Surface-emitting Lasers: Design, Fabrication, Characterization, and Applications, Cambridge University Press, Cambridge, 1999.

[8] H.J. Unold, S.W.Z. Mahmoud, et al., Large-area single-mode selectively oxidized VCSELs: approaches and experimental, Proc. SPIE 3946 (2000) 207–218.

[9] D.L. Huffaker, D.G. Deppe, K. Kumar, T.J. Rogers, Native-oxide defined ring contact for low threshold vertical-cavity lasers, Appl. Phys. Lett. 65 (1994) 97–99.

[10] N. Tansu, L.J. Mawst, Compressively-strained InGaAsP-active ($\lambda = 0.85\,\mu m$) VCSELs, Proc. CLEO 2 (2000) 724–725.

[11] K.D. Choquette, R.P. Schneider Jr., K.L. Lear, K.M. Geib, Low threshold vertical-cavity lasers fabricated by selective oxidation, Electron. Lett. 30 (1994) 2043–2044.

[12] H. Martinsson, J.A. Vukusic, M. Grapbherr, R. Michalzik, R. Jager, K.J. Ebeling, A. Larsson, Transverse mode selection in large-area oxide-confined vertical-cavity surface-emitting lasers using a shallow surface-relief, IEEE Photon. Technol. Lett. 11 (1999) 1536–1538.

[13] H. Unold, S.W.Z. Mahmoud, R. Jager, M. Kicherer, M.C. Riedl, K.J. Ebeling, Improving single-mode VCSEL performance by introducing a long monolithic cavity, IEEE Photon. Technol. Lett. 12 (2000) 939–941.

[14] K.D. Choquette, K.M. Geib, R.D. Briggs, A.A. Allerman, J.J. Hindi, Single transverse mode selectively oxidized vertical cavity lasers, Proc. SPIE 3946 (2000) 230–233.

[15] E.W. Young, K.D. Choquette, S.L. Chuang, K.M. Geib, A.J. Fischer, A.A. Allerman, Single-transverse-mode vertical-cavity lasers under continuous and pulsed operation, IEEE Photon. Technol. Lett. 3 (2001) 927–929.

[16] A.J. Fischer, K.D. Choquette, W.W. Chow, A.A. Allerman, D.K. Serkland, K.M. Geib, High single-mode power observed from a couple-resonator vertical-cavity laser diode, Apply. Phys. Lett. 79 (2001) 4079–4081.

[17] M. Gudent, J. Piprek., Material parameters of quaternary III–V semiconductors for multilayer mirrors at 1.55 μm wavelength,, Modeling Simul. Mater. Sci. Eng. 4 (1996) 349–357.

[18] P.K. Choudhury, O.N. Singh, Some multilayered and other unconventional lightguides, in: O.N. Singh, A. Lakhtakia (Eds.), Electromagnetic Fields in Unconventional Structures and Materials, Wiley, USA, 2000, pp. 289–357.

[19] S.M. Mitani, P.K. Choudhury, M.S. Alias, On the characterization of a new type of oxide confined 850 nm GaAs based vertical cavity surface-emitting laser, Optik (2006) doi:10.1016/j.ijleo.2006.12.007.

[20] S.M. Mitani, M.S. Alias, P.K. Choudhury, Simulation of a new type of oxide confined 850 nm VCSEL, Proc. TENCON2006 00 (2006) TEN264.
[21] S.M. Mitani, M.S. Alias, S.A. Mohammed, K.A. Sharif, P.K. Choudhury, Vertical-cavity surface-emitting laser (VCSEL) in the visible range: modeling, design and analysis, ICSSST (2006) 45–49.
[22] Y. Suematsu, A.R. Adams, Handbook of Semiconductor Lasers and Photonic Integrated Circuits, Chapman & Hall, London, 1994.